Sensitivity enhancement in MAS NMR of half-integer quadrupolar nuclei using sideband selective double-frequency sweeps

M. Goswami, P.J.M. van Bentum, and A.P.M. Kentgens

Abstract: Sensitivity enhancement of the NMR signal of the half-integer spin quadrupolar nuclei under magic angle spinning (MAS) conditions is demonstrated using the DFS (Double Frequency Sweep) enhancement scheme. It has been shown, both through numerical simulations and by experiments, that with a sinusoidal amplitude profile a narrow band DFS scheme performs much better than a DFS scheme with a large bandwidth. The total enhancement compares favorably to the hyperbolic secant (HS) pulse scheme under MAS. Finally, we report the robustness of this DFS scheme with respect to variation of different experimental parameters, making it a very attractive choice for acquiring sensitivity-enhanced NMR experiments of half-integer quadrupolar nuclei.

Key words: quadrupolar nuclei, MAS, double frequency sweeps, adiabatic pulse, CT, ST, sensitivity enhancement.

Résumé : On fait la démonstration d'une méthode d'amélioration de la sensibilité du signal RMN des noyaux quadripolaires de spins non entiers, dans les conditions de rotation à l'angle magique (« MAS »), qui utilise un schéma d'exaltation de balayage à double fréquence (BDF). Il est démontré tant par des calculs théoriques que par des données expérimentales que, avec un profil d'amplitude sinusoïdale, un schéma de BDF avec une bande étroite fonctionne beaucoup mieux qu'un schéma de BDF avec une grande largeur de bande. Dans les conditions de rotation à l'angle magique, l'amélioration totale se compare favorablement au schéma de pulsation sécante hyperbolique (SH). Enfin, on rapporte la force de ce schéma de balayage à double fréquence par rapport à la variation des différents paramètres expérimentaux qui en fait un choix très attrayant pour acquérir des données expérimentales de RMN avec une grande sensibilité pour des noyaux quadripolaires non entiers.

Mots-clés : noyau quadripolaire, rotation à l'angle magique (« MAS »), balayages à double fréquence, pulsation adiabatique, CT, ST, amélioration de la sensibilité.

[Traduit par la Rédaction]

1. Introduction

The application of nuclear magnetic resonance (NMR) to half-integer quadrupolar nuclei is widespread because of their abundant occurrence in various materials of inorganic, catalytic, and biological importance.[1,2] Extracting information about the quadrupolar interactions to which these nuclei are subjected can give valuable insights into the structural and dynamic properties of such compounds. However, the sensitivity of most quadrupolar nuclei (except for instance ^{79}Br or ^{23}Na) is notoriously low because it is affected by several factors such as low natural abundance, small values of gyromagnetic ratios, and large values of quadrupolar interaction parameters. Hence, designing efficient sensitivity enhancement schemes for quadrupolar nuclei still holds the attention of the solid-state NMR community.

In the presence of a static magnetic field, the energy levels of half-integer quadrupolar nuclei split into $2I + 1$ energy levels. At thermal equilibrium, the populations of these energy levels are governed by the Boltzmann distribution. In the high-temperature approximation, the spin levels are populated proportionally to their magnetic quantum number m. Therefore, manipulation of the satellite transitions is a useful tool to increase the polarization of the central transition (CT) levels. A subsequent inversion from the outer to the inner satellite transitions (ST) brings the population from the outer levels into the central transition levels, so that the intensity of NMR spectra of the central transition can be enhanced by a factor of $2I$.

One way to achieve this is by the application of amplitude-modulated pulses, a technique which was pioneered by Vega and Naor.[3] For a spin-3/2 nucleus contained within a single crystal, they had successfully demonstrated that an enhancement of 3 can be obtained by using amplitude-modulated pulses. However, the pulsed approach cannot achieve a similar level of enhancement in powdered samples where the satellite transitions cover a wide frequency range from 0 to $\pm\omega_Q$, where ω_Q represents the quadrupolar frequency.

Received 1 January 2011. Accepted 13 February 2011. Published at www.nrcresearchpress.com/cjc on 25 August 2011.

M. Goswami, P. van Bentum, and A. Kentgens. Radboud University Nijmegen, Institute for Molecules and Materials, Heyendaalsweg 135, 6525 AJ Nijmegen, The Netherlands.

Corresponding author: A.P.M. Kentgens (e-mail: A.Kentgens@nmr.ru.nl).

This article is part of a Special Issue dedicated to Professor Roderick E. Wasylishen.

An attractive alternative approach is to use adiabatic passage schemes. It is known from classic continuous-wave NMR spectroscopy that adiabatic field or frequency sweeps can overcome the problem of a spread in resonance frequencies. The frequency sweep can invert a specific transition by sweeping the frequency of the rf field from far above resonance to far below the resonance condition of the transition under consideration. In-depth studies of the applications of these techniques to half-integer spin quadrupolar nuclei were first made by Haase et al.[5,6] and Kentgens et al.[4,7] Later adiabatic schemes like Double Frequency Sweep (DFS)[8–11] and hyperbolic secant (HS)[12–15] pulse techniques were developed which enhance the sensitivity of quadrupolar nuclei by adiabatically inverting the populations of the outer satellites to the inner ones simultaneously. To date, the DFS scheme with a large sweep range yields the best signal enhancement for the acquisition of NMR spectra of stationary powdered samples with enhancements of up to 2.5 for spin-3/2 nuclei. Similar observations were made by Schurko et al. when they applied the DFS scheme sweeping over a frequency range of ~1.6 MHz observing ^{87}Rb in a static powdered $RbClO_4$ sample.[16] Enhancements ranging from one to two orders of magnitude could be obtained by combining the broad banded DFS with the quadrupolar Carr–Purcell–Meiboom–Gill (QCPMG) pulse sequence for both static and spinning samples.

Under MAS conditions, so far the HS-based inversion results in the largest signal enhancement (up to 2.7 for spin-3/2).[13] In the optimization of the HS pulses, Wasylishen and co-workers found that optimal enhancements are obtained when the bandwidth of the pulse is confined to approximately 1 rotor period.[17] The WURST (wideband uniform-rate smooth truncation)[18] pulse is also associated with large bandwidth to invert the populations of STs and thereby increasing the population differences between CTs.[19] Recently, however, it was reported by Dey et al.[20] that a single WURST inversion pulse under MAS conditions applied to a single satellite transition spinning sideband (ssb) can effectively invert the whole ssb manifold and can achieve appreciable enhancement in the signal to noise ratio for spin-3/2 systems.

Schurko and co-workers explored the optimal control approach to obtain signal enhancements in half-integer spin quadrupolar nuclei under static conditions.[21] These pulses achieved both excitation of the central transition and signal enhancement by population transfer from the satellites. The authors reported enhancements by factors of more than 2 for the central transition of the spin-3/2 ^{87}Rb nucleus compared with a selective $\pi/2$ pulse. These optimized pulses also showed relative insensitivity to the changes made in carrier offset and RF power.

In this contribution, we analyse the behaviour of a narrowband DFS scheme under MAS. We demonstrate a new simple modification to a narrowband DFS scheme which results in greater enhancement than that of normal broadband DFS under MAS. Application of this modified DFS scheme shows enhancements both in numerical simulations as well as in experimental results which are comparable to that of the HS scheme. The new modified scheme, called sideband-selective double-frequency sweep (ssDFS), is obtained by multiplying a narrowband DFS with a sine-squared function. The motivation behind this modification is to reduce the excitation effects by smoothly increasing then decreasing the amplitude of the sweep. We examined the robustness of this scheme with respect to the RF field strength used for the DFS, carrier offset, sweep length, and bandwidth of the DFS. It is shown both numerically and experimentally that ssDFS performs better in terms of total enhancement obtained and is less dependent on experimental parameters.

2. Experimental

The experiments were performed on a Varian NMR System (VNMRS) 300 (7.05 T) and a VNMRS 400 (9.4 T) spectrometer using 2.5 and 3.2 mm HX probe heads. Experiments were performed observing the spin-5/2 ^{27}Al resonance in the Albite, $NaSi_3AlO_8$ sample. The sample was spun at 10 kHz at the magic angle. The quadrupolar coupling constant C_Q and asymmetry parameter η of the ^{27}Al nuclei in Albite were 3.29 MHz and 0.62, respectively.[22] The RF field strength and the duration of the central transition selective 90° pulse applied were 5 kHz and 16.7 μs, respectively.

2.1. DFS

We used a convergent DFS with starting (ω_s) and finishing (ω_f) resonance offsets of 1.1 MHz and 100 kHz, respectively, on the VNMRS 300 spectrometer, whereas the sweep spans from 1 MHz to 100 kHz were carried out on a VNMRS 400 spectrometer. For experiments with DFS having narrow bandwidth, we made use of a convergent DFS with bandwidth equal to the spinning frequency. The other experimental parameters are given in the respective figure captions. For experiments using the ssDFS, we multiplied a convergent DFS, with a bandwidth equalling the spinning frequency, by a sine-squared function (Fig. 1). The sine-squared function was chosen so that the resulting RF profile has a smooth build-up and decay.

2.2. HS pulse

We also made use of HS pulses with a bandwidth of 10 kHz, and offsets of ±160 kHz and ±230 kHz on the VNMRS 300 and 400 spectrometers, respectively. The other relevant pulse and acquisition parameters are given in the figure captions.

2.3. Simulation of NMR spectra using SIMPSON

All the simulations of NMR spectra were carried out using the program SIMPSON (version 3.0.1)[23] running on a Dell Optiplex 755 desktop PC under the Windows XP operating system. The shapes of the DFS and ssDFS amplitude profiles and also the hyperbolic secant pulses were created within the SIMPSON input file. Typically, the powder-averaged spectra were calculated using 4180 crystal orientations using the method of Zaremba, Conroy, and Wolfsberg[24–26] and 10 γ angles. The maximum time step over which the Hamiltonian was considered time independent was 0.5 μs which is also the time step for the DFS and the hyperbolic secant shape. The SIMPSON simulations for a spin-5/2 system with 1000 μs long DFS took around 4 h to finish. All simulations were carried out assuming a spinning frequency of 10 kHz.

3. Results and discussion

Here we present the results obtained from both numerical simulations and experiments done on an Albite ($NaSi_3AlO_8$)

Fig. 1. (*a*) The RF profile of a 900-μs-long narrowband Double Frequency Sweep, (*b*) the $\sin^2 x$ shape function, and (*c*) resultant RF-amplitude profile of a 900-μs-long ssDFS.

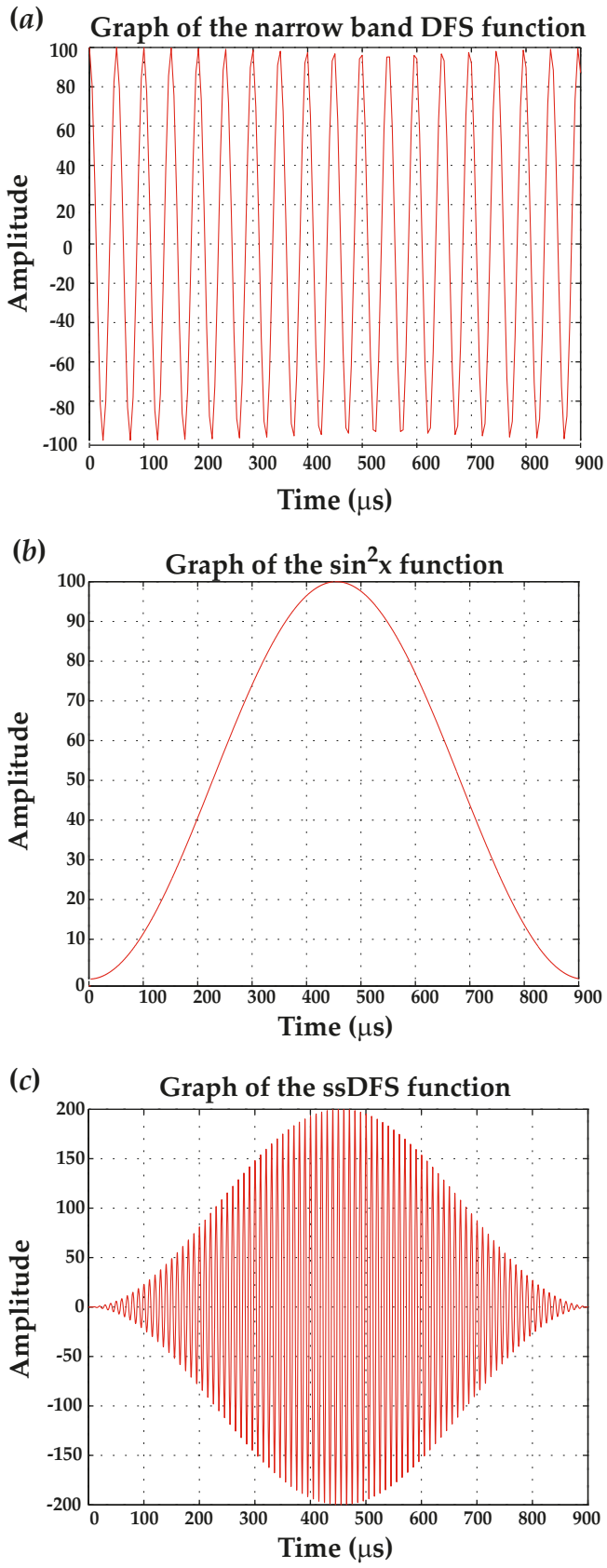

sample at two different external magnetic field strenghts (7.05 T and 9.4 T). We recorded the enhancement factors observed by applying DFS, ssDFS, and HS pulses prior to a selective 90° pulse on the central transition. We also present the behavior of the enhancement factor obtained using ssDFS as a function of different experimental parameters.

3.1. NMR experiments

One-dimensional (1D) MAS spectra of Albite obtained using a single selective 90° pulse, DFS with large bandwidth, DFS with bandwidth equal to the spinning frequency, ν_r, and the sideband-selective DFS are shown in Fig. 2. The experimental results show that the DFS with bandwidth equal to ν_r performs better than normal broadband DFS and the ssDFS performs even better. In the case of the narrowband DFS, the bandwidth was kept equal to ν_r so that the sweep affects only one set of sidebands originating from both ST2 (outer satellite transition) and ST1 (inner satellite transition) on either side of the central transition. Similar observations were made by Wasylishen et al.[17] where they applied adiabatic pulses with bandwidth less than ν_r and conditions were designed such that the sweep only affected one ST (one ST1 and one ST2) sideband on one side of the central transition called SFS (Single Frequency Sweep). They observed that SFS under this condition performs better than normal DFS. Here we observe that if we keep the bandwidth of the DFS equal to ν_r so that it affects the sidebands from both sides of the central transition, the resultant enhancement is still higher than that obtained with a DFS with large bandwidth.

We also implemented HS pulses for ^{27}Al NMR in Albite with a bandwidth equal to 10 kHz. When comparing the results obtained with the HS scheme to that of the ssDFS it turns out that the ssDFS actually performs comparably or even slightly better than that of HS (Fig. 3). Similar results were obtained when these experiments were performed at a 300 MHz spectrometer (data not shown). The enhancement factors are listed in Table 1.

To investigate the robustness of the ssDFS scheme with respect to various experimental settings such as the RF field strength of the DFS, carrier offset, sweep duration, and bandwidth of DFS, we studied the enhancement factor as a function of these variables.

At first we varied the sweep length of the DFS scheme. The enhancement factor displayed a remarkable robustness (Fig. 4*a*). The sweep length was optimized at 1 ms (10 rotor periods) and was varied from 500 μs (5 rotor period) to 1.5 ms (15 rotor period). The enhancement factor shows a flat profile when plotted against sweep length expressed in rotor periods with a maximum observed drop in enhancement by only 8% from its optimum value.

Figure 4*b* shows the signal enhancement factor for the ssDFS scheme plotted as a function of the RF field strength of the DFS, ν_{RF}^{DFS}. The DFS was optimized at an RF field strength of 17.5 kHz, and subsequently varied from 7.5 kHz to 37.5 kHz. The enhancement factor is somewhat lower at the lowest RF field strength building up to its optimum at 17.5 kHz, subsequently displaying a relatively flat profile throughout with a maximum drop of 12% of the enhancement factor from its optimum value.

Figure 4*c* displays the variation of enhancement factor as a function of carrier frequency of the DFS. Here we have var-

Fig. 2. Experimental 1D MAS spectra of ^{27}Al nuclei in Albite sample obtained on a VNMRS 400 spectrometer under different pulse schemes: (*a*) selective 90° pulse, (*b*) DFS running from 1.0 MHz to 100 kHz, (*c*) narrowband DFS running from 230 kHz to 220 kHz, (*d*) ssDFS. The numbers on the right of each spectrum denote the associated enhancements. The RF on ^{27}Al during DFS was kept at 17.5 kHz and that of central-transition selective 90° pulse was 5 kHz. The sweep duration was optimized to 1000 μs to obtain maximum signal intensity. A total of 64 transients were acquired with a relaxation delay of 2 s.

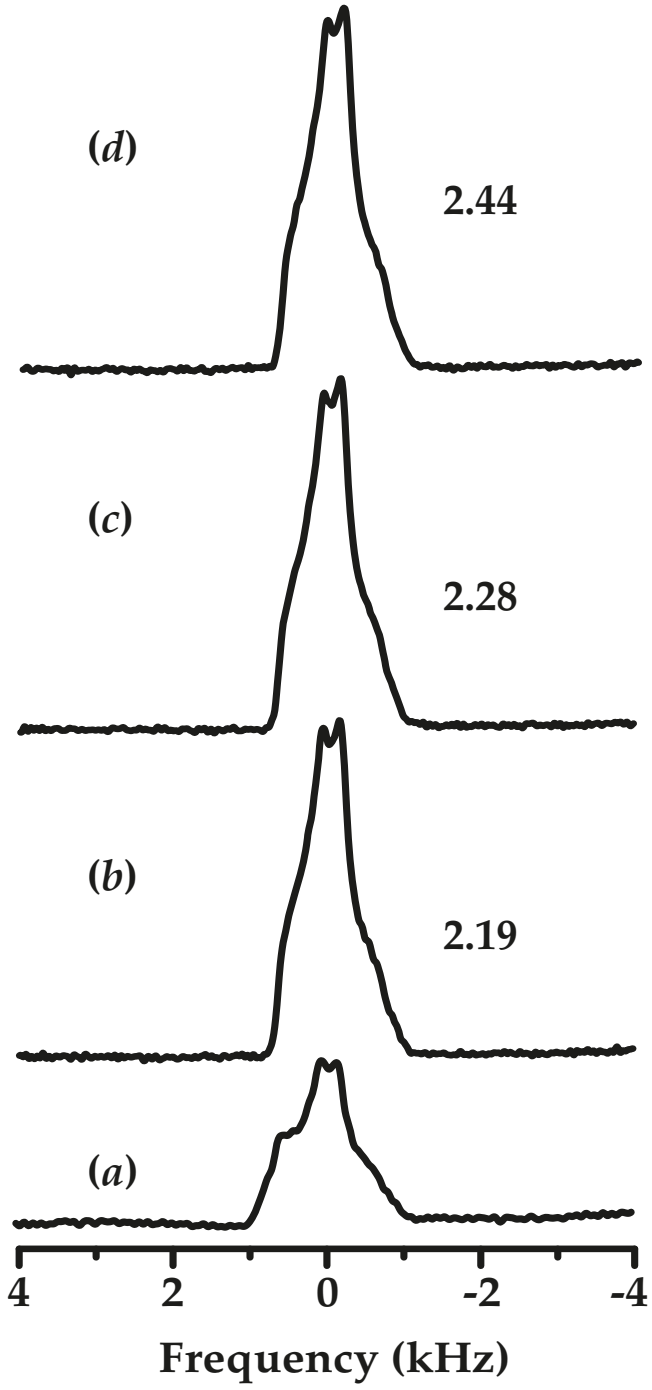

ied the position of the transmitter from the center of the central transition peak to ±100 kHz on either side of the center so that the DFS operates asymmetrically around the central

Fig. 3. Experimental 1D MAS spectra of ^{27}Al nuclei on a VNMRS 400 spectrometer using different pulse schemes: (*a*) selective 90°, (*b*) hyperbolic secant pulse, (*c*) ssDFS. The numbers on the right of each spectrum denote the associated enhancements. The HS pulse had an offset of ± 230 kHz and bandwidth of 10 kHz. The duration of the HS pulse was 2050 μs at an RF of 17.5 kHz. The RF field strength of the central-transition selective 90° pulse was 5 kHz. The number of transients and the relaxation delay time were the same asfor the DFS experiment.

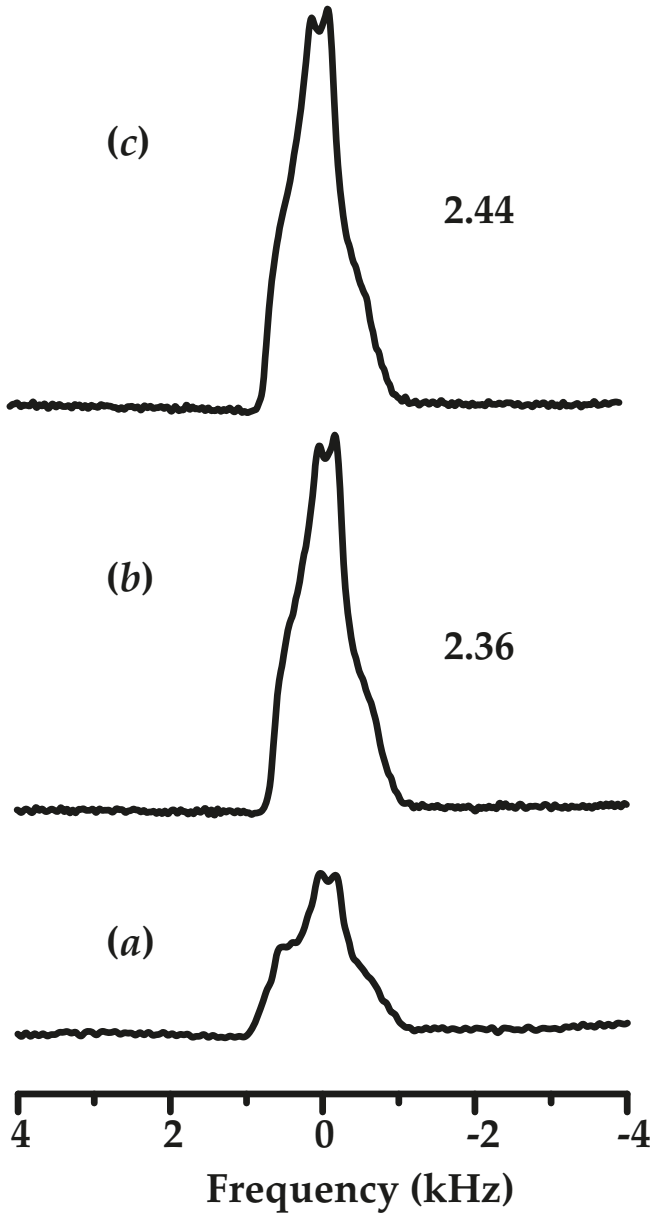

transition peak. Again, the plot of the enhancement factor versus carrier offset shows a remarkably flat profile between ±50 kHz of carrier offset. Only after ±50 kHz does the enhancement factor start to show a small decline. Again, the maximum drop in the enhancement factor was only ~8% from the optimum value.

Next we varied the bandwidth of the ssDFS from 5 kHz to 20 kHz i.e., 1/2 to 2 times spinning frequency. Interestingly, the enhancement factor now shows an oscillatory behavior

Table 1. Experimental enhancements obtained with respect to a selective 90° pulse, using different enhancement schemes at two different magnetic fields for ^{27}Al nuclei in the Albite sample.

Magnetic field	Broadband DFS	Narrowband DFS	HS	ssDFS
7.05 T	2.17±0.02	2.27±0.02	2.32±0.01	2.37±0.01
9.4 T	2.19±0.02	2.28±0.01	2.36±0.01	2.44±0.01

Fig. 4. Simulated and experimental variation of the optimized ^{27}Al NMR signal for a spinning Albite sample at 9.4 T (*a*) as a function of the sweep length (expressed in terms of rotor periods) of the DFS, (*b*) as a function of the RF field strength of the DFS, ν_{RF}^{DFS}, (*c*) as a function of the carrier offset of the DFS, (*d*) as a function of the bandwidth of the DFS.

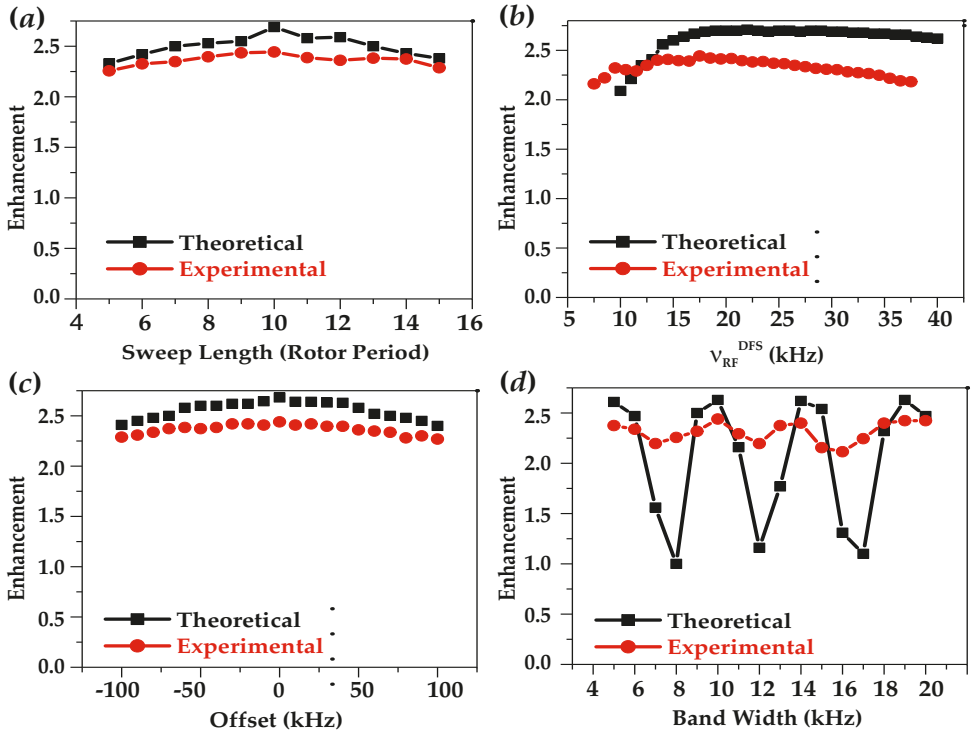

with respect to the variation of the bandwidth (Fig. 4*d*). Incidentally, similar observations were previously made by Wasylishen et al. in the case of hyperbolic secant pulses.[15] Their oscillation frequency, however, was different from ours. When we tried to rationalize this observation, we found that each and every minimum in the plot of enhancement versus bandwidth occurs when the sweep finishes on top of the spinning sidebands (ssb) of either ST1 or ST2. But when the sweep covers an entire ssb of either the inner or outer satellite transitions, the enhancement factor goes up. Hence, it can be said that when the sweep ends on top of an ssb it interferes with the inversion of that ssb which results in a cascading effect on the whole of the ssb manifold leading to smaller enhancements.

In summary, we have shown here that a narrowband DFS scheme performs much better than a broadband DFS for spinning samples. This observation confirms previous observations that narrowband adiabatic methods are best under MAS conditions.[17,20] The various adiabatic schemes perform similarly in terms of the overall enhancement effect. Small differences are attributed to the approach used to avoid *sudden* changes in the spin Hamiltonian causing unwanted excitations of the spin system. Here we have implemented a squared sinusoidal amplitude envelop to the DFS to ensure a smooth increase and decrease of the amplitude at the beginning and end of the sweep. This appears to give slightly better performance compared to other adiabatic schemes. Another favourable aspect of this DFS implementation is the robustness of its performance with respect to a great number of experimental parameters. Considering the fact that a broadband DFS is also the method of choice for enhancing the central-transition powder patterns in static samples, we argue that the DFS is the most versatile implementation for enhancing spectra of half-integer quadrupolar spins. The DFS can easily be implemented in a flexible way so that the bandwidth can be tuned to a small value for spinning conditions, whereas it can be used with a broad bandwidth under static conditions. Slowly building up and bringing down the amplitude of the sweep will avoid excitation effects. The versatility and robustness of this scheme requires very little optimization during actual experiments.

3.2. SIMPSON simulations

To validate the effect of ssDFS on the enhancement factor, we performed SIMPSON simulations on a spin-5/2 system using the quadrupolar parameters of ^{27}Al in Albite. It turned out that the simulations provided us with similar observations to those we previously made experimentally. The numerical

Fig. 5. Simulated 1D MAS spectra of ^{27}Al nuclei in Albite with quadrupolar coupling constant C_Q and asymmetry parameter η equal to 3.29 MHz and 0.62, respectively, using different pulse schemes. (*a*) A single 90°, (*b*) DFS running from 900 kHz to 100 kHz, (*c*) DFS running from 170 kHz to 160 kHz, (*d*) ssDFS. The numbers on the right of each spectrum denote the associated signal enhancements with respect to the single-pulse experiment.

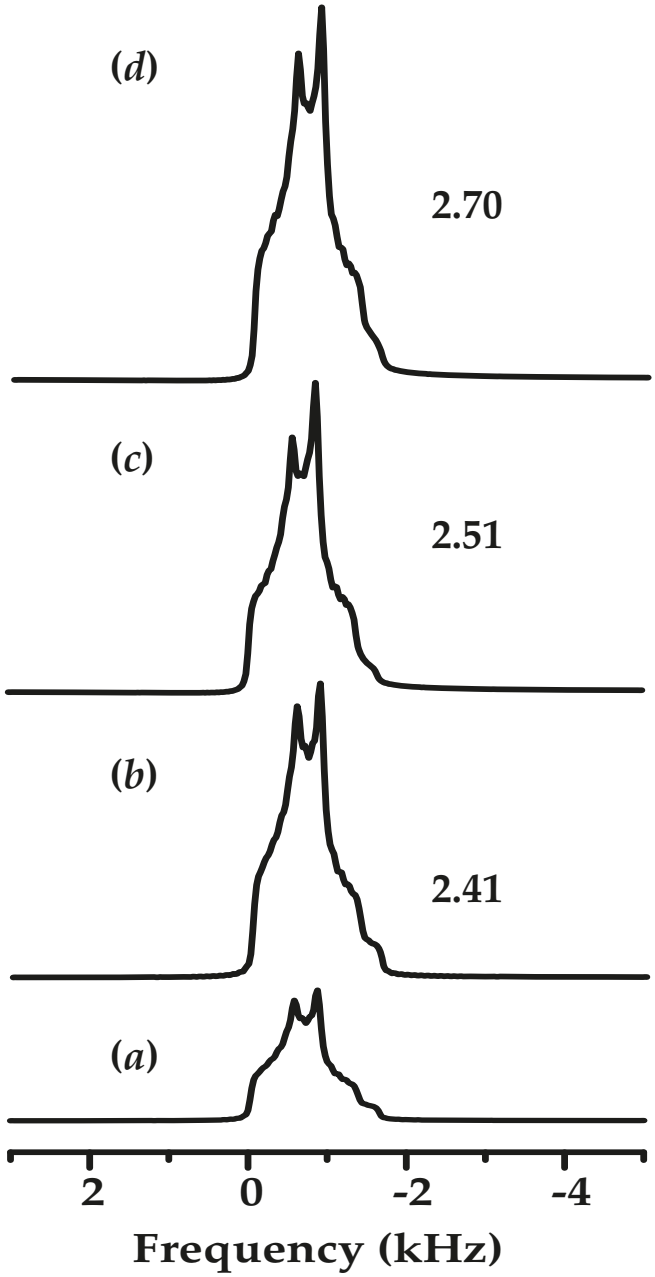

simulations show that the DFS with bandwidth equal to MAS rate, ν_r, should perform better than normal DFS whereas the ssDFS should perform even better (Fig. 5). When we further compared the ssDFS with the HS pulse, it turned out that in simulations as in experiments they behave comparably to each other (Fig. 6). Similar observations were made when we did numerical simulations for spin-3/2 and spin-7/2 systems. The results are given in Table 2. For simulations of a spin-3/2 system, we used the quadrupolar parameters of ^{87}Rb in $RbClO_4$ (C_Q = 3.29 MHz and η = 0.2) and for a spin-7/2

Fig. 6. Simulated 1D MAS spectra of ^{27}Al in Albite. (*a*) A single 90°, (*b*) hyperbolic secant pulse, and (*c*) ssDFS. The numbers on the right of each spectrum denote the associated enhancements with respect to the single-pulse experiment.

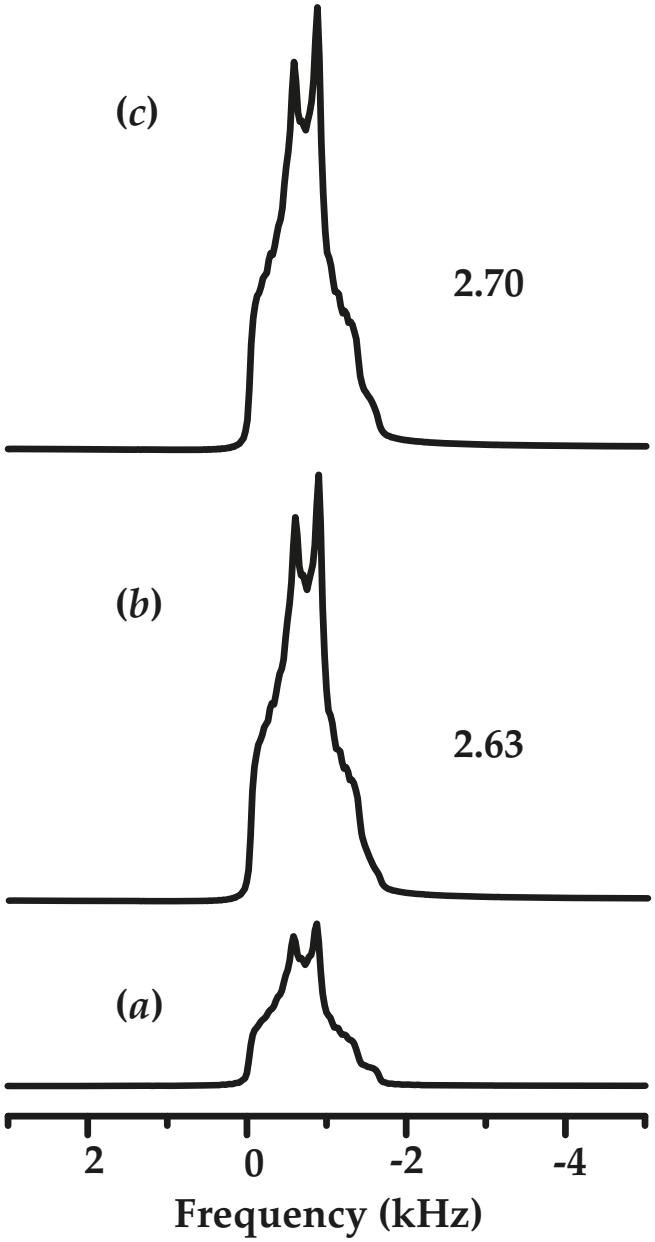

system we used the quadrupolar parameters of ^{43}Ca in $CaTiO_3$ (C_Q = 2.13 MHz and η = 0.7). The data indicate that the ssDFS scheme is universally applicable to all nuclei with half-integer quadrupolar spins.

Next we simulated the robustness of the enhancement factor obtained by the ssDFS scheme as a function of the variables such as RF field strength, sweep length, bandwidth, and carrier offset of the ssDFS scheme.

At first, we varied the length of the ssDFS. As in the experiments, the optimum sweep length was equal to 10 rotor periods i.e., 1000 μs, and was varied from the 5th to the 15th rotor period. As in the experimental results, the enhancement factor shows significant robustness with respect to the change of the sweep length(Fig. 4*a*). Next we plotted

Table 2. Simulated optimal enhancements obtained with respect to a single 90° pulse at 10 kHz MAS, using different enhancement schemes for $I = 3/2$, 5/2, and 7/2 spin systems. The quadrupolar parameters of ^{87}Rb ($I = 3/2$) in $RbClO_4$ ($C_Q = 3.2$ MHz and $\eta = 0.21$), ^{27}Al ($I = 5/2$) in Albite ($C_Q = 3.29$ MHz and $\eta = 0.62$), and ^{43}Ca ($I = 7/2$) in $CaTiO_3$ ($C_Q = 2.13$ MHz and $\eta = 0.7$) were chosen as model parameters in the simulations.

Spin system(I)	Broadband DFS	Narrowband DFS	HS	ssDFS
Spin-3/2	2.25	2.45	2.58	2.60
Spin-5/2	2.41	2.51	2.63	2.70
Spin-7/2	3.19	3.41	3.55	3.64

the variation of the enhancement factor as a function of the RF power of the DFS, ν_{RF}^{DFS}. It is evident from the plot that as in the experimental findings, the simulated enhancement factor shows an initial fast build-up as a function of ν_{RF}^{DFS}, then flattens and remains flat almost throughout the range of the plot (Fig. 4*b*). The theoretical variation of the enhancement factor as a function of carrier frequency of the DFS is shown in Fig. 4*c*. Here we mimicked the experimental condition by changing the position of the transmitter from the center of the central transition to ±100 kHz on either side of the center with an increment of 10 kHz, so that the sweep is asymmetrical around the central transition peak. It is clear from the plot that the profile of the enhancement factor remains essentially flat throughout the whole range, showing very little dependence on the variation of the carrier offset. An observation which is again similar to the experimental observation.

Next, as we varied the bandwidth of the ssDFS, we observed that here as well the simulated results follow the experimental results and the enhancement factor shows an oscillating behavior when the bandwidth is varied (Fig. 4*d*). Further, the oscillation frequency of the simulated plot remains almost identical to that of the experimental plot. However, one clear difference between the simulated and experimental plots is that the experimental oscillation displays much more damping than the simulated one. One possible reason could be the finite line widths of the experimental ssbs. This means that experimentally it may not be possible to end the sweep exactly on top of an ssb, resulting in damped oscillation.

4. Conclusions

In this report, we have provided both theoretical and experimental proof that a narrowband DFS scheme performs better than a normal broadband DFS under MAS for spin $I = 5/2$. In general, adiabatic pulses focussing on the inversion of a single sideband seem to perform best in inverting the whole sideband manifold. Subtle differences between these adiabatic schemes are attributed to differences in the amplitude profiles applied to avoid unwanted non-adiabatic excitations of the spin system. The DFS scheme possesses the flexibility to be used with a narrow bandwidth for spinning samples as well as with a large bandwidth for static samples. Further, it has been shown that the enhancement obtained with an ssDFS scheme is actually comparable with that obtained with hyperbolic secant scheme. Simulations for spin $I = 3/2$ and $I = 7/2$ indicate that the advantages of the ssDFS scheme are applicable across the whole range of half-integer spin-quantum numbers. An additional increase in the signal may be obtained by using repetitive ssDFS as has been shown using multiple RAPT,[27] repetitive DFS,[28] and multiple FAM experiments.[29] The robustness of the ssDFS scheme with respect to the (peak) RF field strength of the DFS, carrier offset, and sweep duration of the DFS has also been demonstrated. All these observations display the broad applicability of the DFS method which can be optimized once and used for all purposes. It is expected that the combination of desirable features such as higher enhancement, robustness, and the ease of implementation associated with the ssDFS scheme will make the application of this method more routine.

Acknowledgements

This work has been supported by EuroMagNET under the EU contract no 228043. We also acknowledge the support of the Netherlands Organisation for Scientific Research NWO for support of the Solid State NMR Facility for advanced materials science. We are grateful to the technical staffmembers G. Janssen, Hans Janssen, and J. van Os for their technical support.

References

(1) MacKenzie, K. J. D.; Smith, M. E. *Multinuclear Solid-State NMR of Inorganic Materials*; Pergamon Press, Oxford, 2002.
(2) Yamauchi, K.; Kuroki, S.; Ando, I.; Ozaki, T.; Shoji, A. *Chem. Phys. Lett.* **1999** *302* (3-4), 331. doi:10.1016/S0009-2614(99)00127-X.
(3) Vega, S.; Naor, Y. *J. Chem. Phys.* **1981** *75* (1), 75. doi:10.1063/1.441857.
(5) Haase, J.; Conradi, M. S. *Chem. Phys. Lett.* **1993** *209* (3), 287. doi:10.1016/0009-2614(93)80109-3.
(6) Haase, J.; Conradi, M. S.; Grey, C. P.; Vega, A. J. *J. Magn. Reson. A* **1994** *109* (1), 90. doi:10.1006/jmra.1994.1138.
(4) Kentgens, A. P. M. *J. Magn. Reson.* **1991** *95*, 619.
(7) van Veenendaal, E.; Meier, B. H.; Kentgens, A. P. M. *Mol. Phys.* **1998** *93*, 195. DOI: 10.1080/002689798169212.
(8) Kentgens, A. P. M.; Verhagen, R. *Chem. Phys. Lett.* **1999** *300* (3–4), 435. doi:10.1016/S0009-2614(98)01402-X.
(9) Iuga, D.; Schäfer, H.; Verhagen, R.; Kentgens, A. P. M. *J. Magn. Reson.* **2000** *147* (2), 192. doi:10.1006/jmre.2000.2192.
(10) Schäfer, H.; Iuga, D.; Verhagen, R.; Kentgens, A. P. M. *J. Chem. Phys.* **2001** *114* (7), 3073. doi:10.1063/1.1340576.
(11) Iuga, D.; Kentgens, A. P. M. *J. Magn. Reson.* **2002** *158* (1–2), 65. doi:10.1016/S1090-7807(02)00061-7.
(12) Siegel, R.; Nakashima, T. T.; Wasylishen, R. E. *Chem. Phys. Lett.* **2004** *388* (4–6), 441. doi:10.1016/j.cplett.2004.03.047.
(13) Siegel, R.; Nakashima, T. T.; Wasylishen, R. E. *Concepts Magn. Reson.* **2005** *26A* (2), 47. doi:10.1002/cmr.a.20037.

(14) Siegel, R.; Nakashima, T. T.; Wasylishen, R. E. *Chem. Phys. Lett.* **2006** *421* (4-6), 529. doi:10.1016/j.cplett.2006.01.107.
(15) Siegel, R.; Nakashima, T. T.; Wasylishen, R. E. *J. Magn. Reson.* **2007** *184* (1), 85. doi:10.1016/j.jmr.2006.09.007.
(16) Schurko, R. W.; Hung, I.; Widdifield, C. M. *Chem. Phys. Lett.* **2003** *379* (1-2), 1. doi:10.1016/S0009-2614(03)01345-9.
(17) Nakashima, T. T.; Wasylishen, R. E.; Siegel, R.; Ooms, K. J. *Chem. Phys. Lett.* **2008** *450* (4–6), 417. doi:10.1016/j.cplett.2007.11.032.
(18) Kupce, E.; Freeman, R. *J. Magn. Reson. A* **1995** *115* (2), 273. doi:10.1006/jmra.1995.1179.
(19) Bhattacharyya, R.; Frydman, L. *J. Chem. Phys.* **2007** *127* (19), 194503. doi:10.1063/1.2793783.
(20) Dey, K. K.; Prasad, S.; Ash, J. T.; Deschamps, M.; Grandinetti, P. J. *J. Magn. Reson.* **2007** *185* (2), 326. doi:10.1016/j.jmr.2006.12.013.
(21) O'Dell, L. A.; Harris, K. J.; Schurko, R. W. *J. Magn. Reson.* **2010** *203* (1), 156. doi:10.1016/j.jmr.2009.12.016.
(22) Kirkpatrick, R. J.; Kinsey, R. A.; Smith, K. A.; Henderson, D. M.; Oldfield, E. *Am. Mineral.* **1985** *70*, 106.
(23) Bak, M.; Rasmussen, J. T.; Nielsen, N. C. *J. Magn. Reson.* **2000** *147* (2), 296. doi:10.1006/jmre.2000.2179.
(24) Zaremba, S. K. *Ann. Mat. Pura Appl.* **1966** *73*, 293. DOI: 10.1007/BF02415091.
(25) Conroy, H. *J. Chem. Phys.* **1967** *47* (12), 5307. doi:10.1063/1.1701795.
(26) Cheng, V. B.; Suzukawa, H. H., Jr; Wolfsberg, M. *J. Chem. Phys.* **1973** *59* (8), 3992. doi:10.1063/1.1680590.
(27) Kwak, H.-T.; Prasad, S.; Clark, T.; Grandinetti, P. J. *Solid State Nucl. Magn. Reson.* **2003** *24* (2–3), 71. doi:10.1016/S0926-2040(03)00051-1.
(28) Brinkmann, A.; Kentgens, A. P. M. *J. Phys. Chem. B* **2006** *110* (32), 16089. doi:10.1021/jp062809p.
(29) Goswami, M.; Madhu, P. K. *J. Magn. Reson.* **2008** *192* (2), 230. doi:10.1016/j.jmr.2008.02.020.